Intermetallics 114 (2019) 106610

Contents lists available at ScienceDirect

Intermetallics

journal homepage: www.elsevier.com/locate/intermet

Cooling rate as a tool of tailoring structure of Fe-(9–33%)Ga alloys

I.S. Golovin[a,*], A.M. Balagurov[b,c], I.A. Bobrikov[b], S.V. Sumnikov[b], A.K. Mohamed[a]

[a] National University of Science and Technology "MISIS", Leninsky Ave. 4, 119049, Moscow, Russia
[b] Frank Laboratory of Neutron Physics, Joint Institute for Nuclear Research, 141980, Dubna, Russia
[c] Lomonosov Moscow State University, 119991, Moscow, Russia

ARTICLE INFO

Keywords:
Functional alloys
Annealing
Metastable phases
Ordering
Phase transformation kinetics
Neutron diffraction

ABSTRACT

A huge difference between the structure and the properties of *equilibrium* and *metastable* Fe–Ga alloys along with an uncertain specification for their metastable state lead to urgent necessity of understanding the cooling rate role in the formation of the alloys structure. We studied structure of Fe-(9-33 at.%)Ga alloys after cooling with different cooling rates (furnace, air, water, as cast) and report structure and dependencies of lattice parameter for A2 and $D0_3$ phases on Ga content in Fe–Ga alloys. The first and second critical cooling rates are determined as the beginning and the end of formation of equilibrium $L1_2$ phase.

1. Introduction

Fe–Ga alloys, also known as Galfenols, exhibit an attractive combination of magnetostrictive and mechanical properties. The puzzle of the nature of giant magnetostriction in ferromagnetic α-Fe alloyed by nonmagnetic Ga is under extensive discussions [1–7]. Magnetostriction of α-Fe increases with an increase in the Ga content in α-Fe-Ga alloys with the A2 structure up to 17–20%Ga (in this paper we use only atomic per cents), then decreases between 20 and 23–24%Ga, again increases between 24 and 27–28%Ga, and finally decreases above 28%Ga. According to the equilibrium phase diagrams [8–10], the alloys with 21–26%Ga correspond to two-phase structures with a mixture of A2 and $L1_2$ crystalline lattices, the alloys with 27–28%Ga correspond to an $L1_2$ single phase, and the alloys with more than 29%Ga correspond to $L1_2$ and Fe_6Ga_5 phases. This statement is also supported by first-principle simulations [11]. Among above mentioned structures, only the A2 phase has positive magnetostriction. Therefore, the real structure of Fe–Ga alloys, in most cases – as cast alloys, is rather different to that of proposed by the equilibrium diagram. Some compromise was found in the paper by O. Ikeda et al. [12], in which a metastable phase diagram was suggested, and it proposes the presence of the $D0_3$ structures with positive magnetostriction – a weakly ordered A2 phase – in a wide range of Ga concentrations in iron. Unfortunately, the term '*metastable*' diagram was not specified with respect neither to cooling rates of the samples nor their size. An increase in the size of bulk materials obviously decreases the cooling rate and leads do a different structure in outer and inner parts of a sample.

The effect of the structure of the Fe–Ga alloys on their functional properties is discussed in almost all research papers, and a huge difference in sample properties after 'quick' and 'slow' cooling is firmly stated. Surprisingly, in almost all papers, the terms 'quick' and 'slow' are not defined with respect to cooling rates.

Earlier, we studied phase transitions in as cast bulk Fe–Ga alloys at instant heating [13,14] and isothermal annealing [15,16] using *in situ* and high resolution neutron diffraction (ND). In this paper, we present the results of structural studies by high resolution ND of bulk samples of Fe-(15–33)Ga alloys cooled down by several regimes. Namely, for all the samples these regimes are: (i) as cast (average cooling rate is estimated to be ~2000 K/min for an ingot with dimensions 60 × 12 × 4 mm), (ii) air cooled (60–70 K/min for a sample with dimensions 30 × 8 × 4 mm), and (iii) furnace cooling (2 K/min for a sample with dimensions 30 × 8 × 4 mm). We also used water quenching but no difference was found between water quenching and as cast samples.

Casting, water-, air- and furnace-cooling are the main regimes for cooling in practice. Our estimations of the cooling rates provide average values for the surface of the samples. The cooling rate of the bulk samples is not linear, and it slows down with a decrease in temperature. For example, the cooling rate of 2 K/min in a vacuumed furnace used for *in situ* neutron diffraction tests is linear between 900 and 250 °C, below 250 °C the cooling rate becomes slower. Nevertheless, the phase transitions below 250 °C are very slow [17] and can be neglected. In addition to above mentioned cooling regimes, we also applied different cooling rates (from 1 to 30 K/min) in order to find out critical cooling rates with respect to formation of equilibrium phases: V_{Cr1} is defined in this paper as the beginning and V_{Cr2} – as the end of formation of

* Corresponding author. Leninsky ave. 4, 119049, Moscow, Russia.
E-mail address: i.golovin@misis.ru (I.S. Golovin).

https://doi.org/10.1016/j.intermet.2019.106610
Received 21 July 2019; Received in revised form 10 September 2019; Accepted 10 September 2019

equilibrium $L1_2$ phase in Fe_3Ga type alloy.

2. Material and methods

Fe-(9-33 at.%)Ga alloys were produced by rapid solidification in a copper mold using Fe (commercial purity) and Ga (99.99%) by induction melting under the protection of a high-purity argon gas in an Indutherm MC–20 V furnace. The chemical compositions were confirmed with an accuracy of 0.2% by Energy Dispersive X-ray Spectroscopy (EDX). In this paper we use only atomic %. For neutron experiments, 4 × 8 × 50 mm parallelepipeds were cut from ingots.

To study the alloy structures after different cooling regimes, the neutron diffraction patterns were measured at a high-resolution Fourier diffractometer (HRFD) [18], operating at the IBR-2 pulsed reactor at JINR (Dubna). This is a time-of-flight (TOF) instrument that can be easily switched between high-resolution ($\Delta d/d \approx 0.0015$) and high-intensity ($\Delta d/d \approx 0.015$) diffraction modes, which are both used for obtaining the data about phase transformations of the alloys [19].

3. Results and discussion

All the studied *as cast* Fe–Ga alloys have metastable structures at room temperature: either A2 (Fig. 1a) or $D0_3$ (Fig. 1b, c and d). $D0_3$ ordering of the A2 structure is detected by appearance of superstructure reflections 111_{D03} and 311_{D03}, which are forbidden in the disordered state.

Fig. 2 summarize the type of structure and corresponding lattice parameter for Fe–Ga alloys with Ga content from 15 to 33 at.%Ga for three cooling regimes: in the as cast state (a), after cooling in air from 950 °C (b), and furnace cooling with 2 K/min (c).

Our results for the *as cast* Fe–Ga samples presented in Fig. 2a (the average cooling rate from the liquid phase is about 2000 K/min) are in an excellent agreement with the data from synchrotron reported in paper [3], where three-ranges dependence was obtained, but not with paper [20], where a monotonous dependence of the lattice parameter is reported. In our study, we used a wider range of Ga concentrations, and this helps us distinguish three intervals in 'lattice parameter *vs* Ga' and four intervals by structure types. Comprehensive results for the Fe–Ga structures after air cooling and furnace cooling (Fig. 2b and c, correspondingly) have no analogous in literature and, thus, they are presented here for the first time.

According to their structure, the as cast samples can be divided into four groups (Fig. 2a):

1 $x < 20$, A2 structure.
2 $20 < x < 27$, A2 as a matrix with $D0_3$ clusters embedded into the matrix (existence of small amount of B2 clusters is also not excluded).
3 $27 < x < 31$, $D0_3$ and B2 structures.
4 $x > 31$, B2 or $D0_3$ plus a phase with unresolved structure.

Within the second group, two subgroups can be distinguished:

2a $21 < x < 23$, lattice parameter and width of fundamental peaks decrease.
2b $23 < x \leq 27$, lattice parameter increases linearly while the intensity of superstructure peak (111) increases, reaches maximum, and decreases.

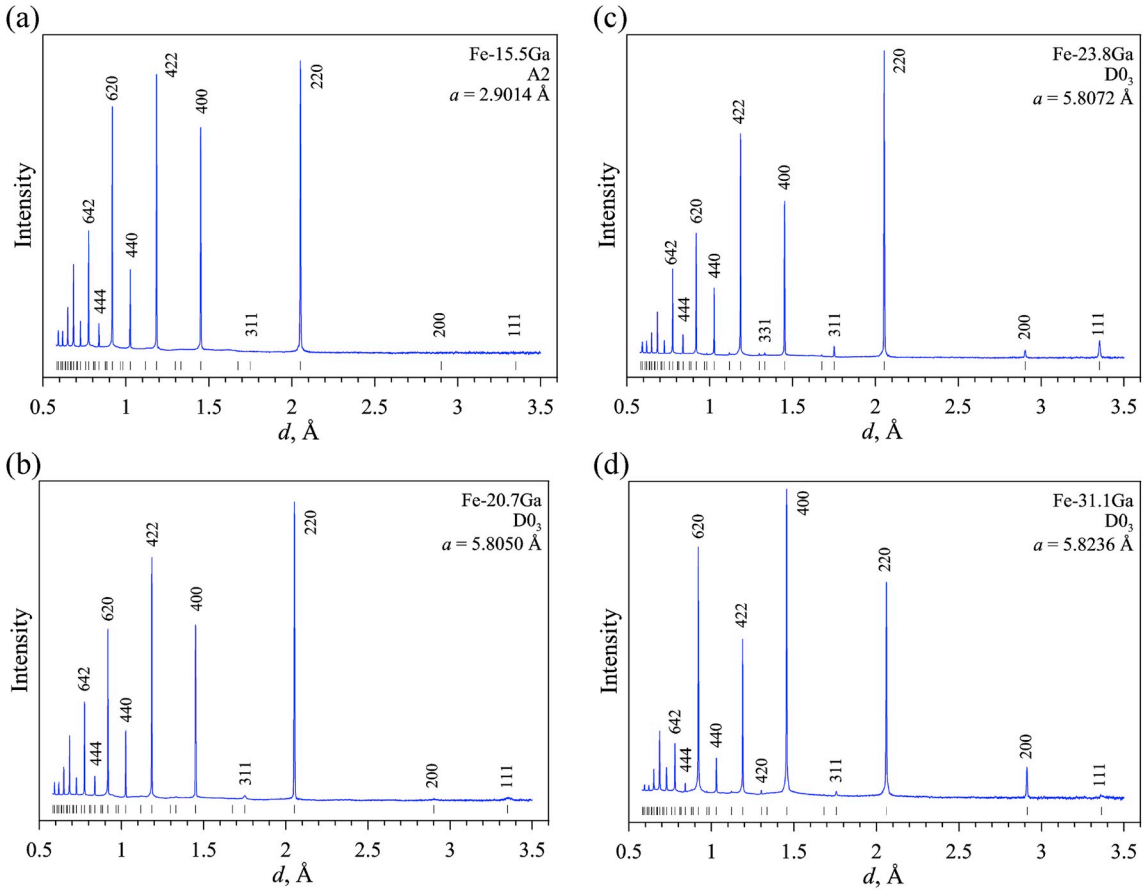

Fig. 1. Neutron diffraction patterns for four as cast Fe-*x*Ga alloys with x = 15.5, 20.7, 23.8 and 31.1 at.% Ga (a), (b), (c) and (d) respectively. Superstructure peaks with odd Miller indices are absent for x = 15.5, start to appear for x = 20.7, are intensive and well formed for x = 23.8, start to go down for x = 31.1.

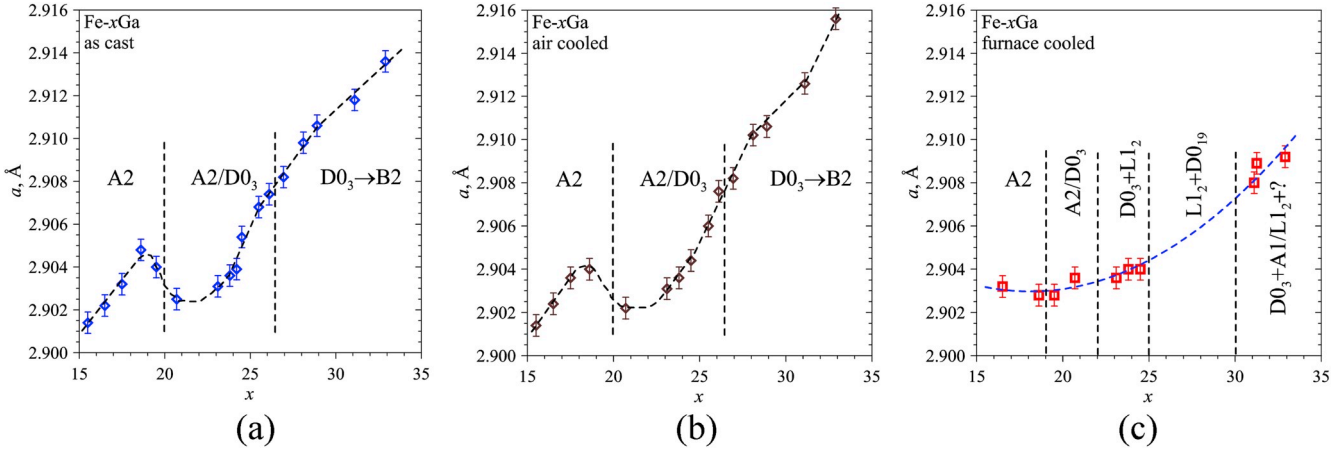

Fig. 2. Lattice parameter of the A2 or $D0_3$ ($á = a/2$) phases for the Fe-xGa alloys with x from 15.5 to 32.9%Ga in the as cast state (a), air cooled (b), and furnace cooled with 2 K/min (c). For the furnace-cooled samples, the A2 and $D0_3$ phases are absent in a range of $26 < x < 30$. Lattice parameters for the closed packed structures ($L1_2$ and $D0_{19}$) are not shown in this figure. The lines are a guide for eyes.

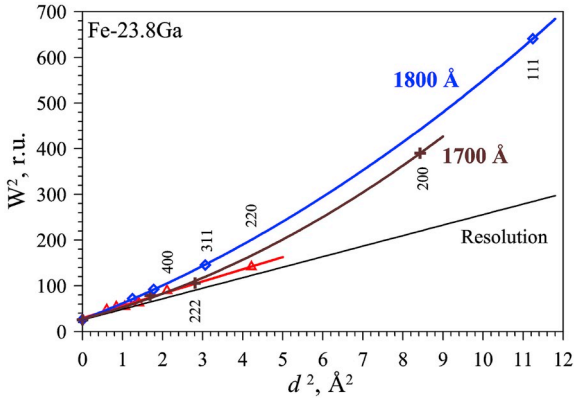

Fig. 3. Williamson-Hall plots for the widths of fundamental diffraction peaks (red triangles), superstructure peaks allowed in the B2 phase (brown crosses), and superstructure peaks allowed in the $D0_3$ phase (blue diamonds). The Miller indices of several first peaks and the characteristic size of clusters are specified. The bottom line shows the diffractometer resolution function. (For interpretation of the references to colour in this figure legend, the reader is referred to the Web version of this article.)

From the viewpoint of the lattice parameter, there is no pronounced difference between the samples in the *as cast* state and the samples cooled down in water, and there is only small difference for the samples with 18.5 and 33%Ga cooled down in open air (Fig. 2a and b). The inflection in the behavior of the lattice parameter above 18.5%Ga is well known for metallic alloys as an effect of ordering: in the ordered state, the lattice is somewhat contracted. The interesting point is that these dependences are obtained from the positions of fundamental peaks, i.e., for the matrix. As follows from the diffraction patterns, up to $x = 20.7$, only the A2 phase is present in the samples, but the dependence $a(x)$ deviates from linear already starting with $x = 18.5$, i.e., the lattice parameter is more sensitive to the beginning of the ordering process than the peak intensities. Up to $x \approx 27$, the ordered clusters occupy a relatively small volume as compared to the volume of a disordered matrix, and it would be reasonable to assume that while the volume of the clusters is small, the lattice parameter of the matrix should change linearly with an increase of the Ga concentration. The deviation from the linear dependence, observed already starting above 18.5%Ga, means that the matrix "adjusts" to the clusters and a high degree of coherence between the lattices of the matrix and the clusters remains.

A more detailed analysis of the data shows that some difference in

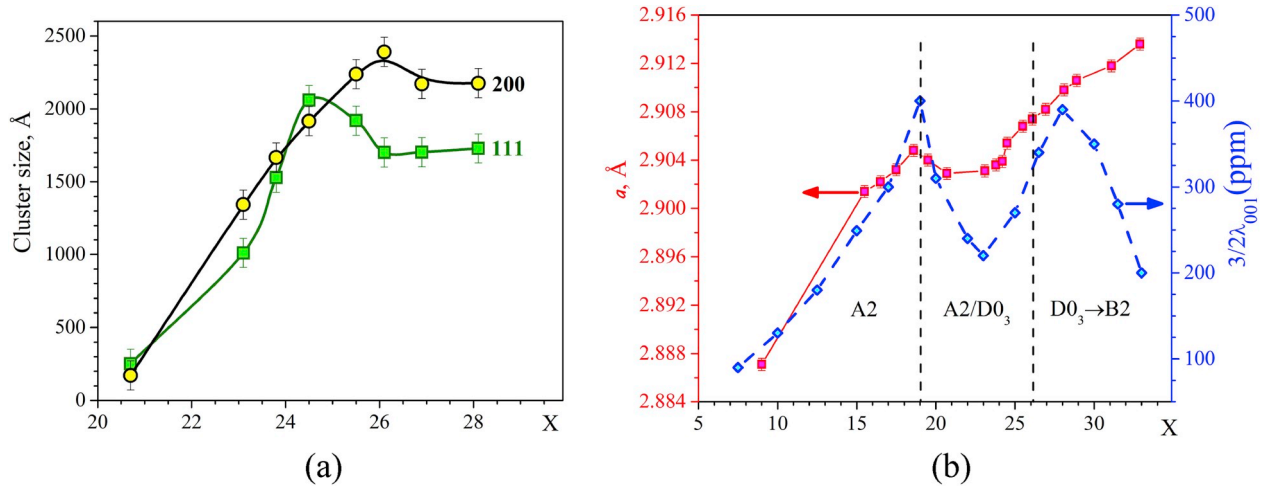

Fig. 4. The average size of clusters with ordered atomic structure determined according to the Scherrer equation from the widths of 111 and 200 superstructure peaks for the Fe-xGa alloys with x from 20.7 to 28.1% (a), and lattice parameter of the A2, B2 or $D0_3$ ($á = a/2$) phases for x from 9 to 32.9%Ga (left scale) and magnetostriction for water quenched Fe–Ga alloys from Ref. [22].

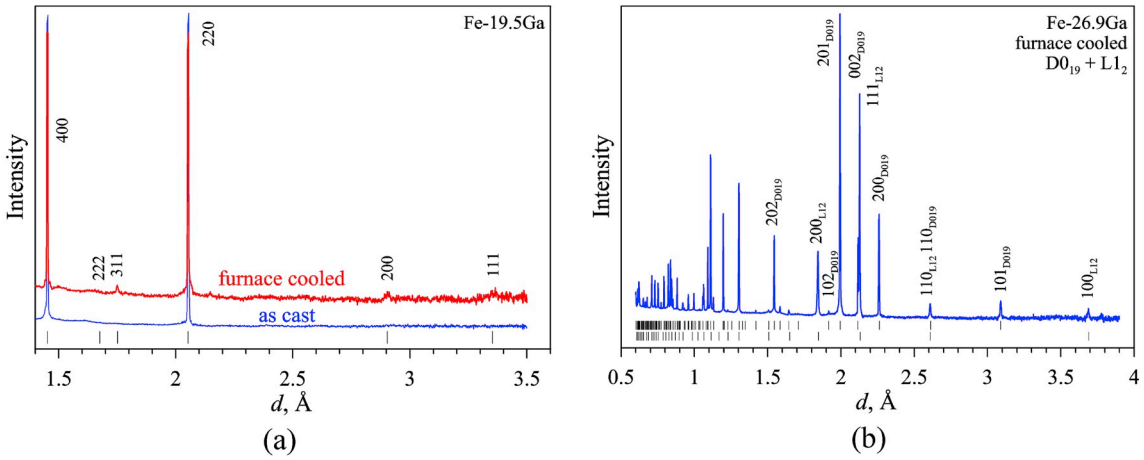

Fig. 5. High resolution neutron diffraction patterns of the Fe-19.5Ga (a) and Fe-26.9Ga (b) alloys after furnace cooling. For Fe-19.5Ga it is compared with the pattern measured in the as cast state. The Miller indices of several peaks are specified.

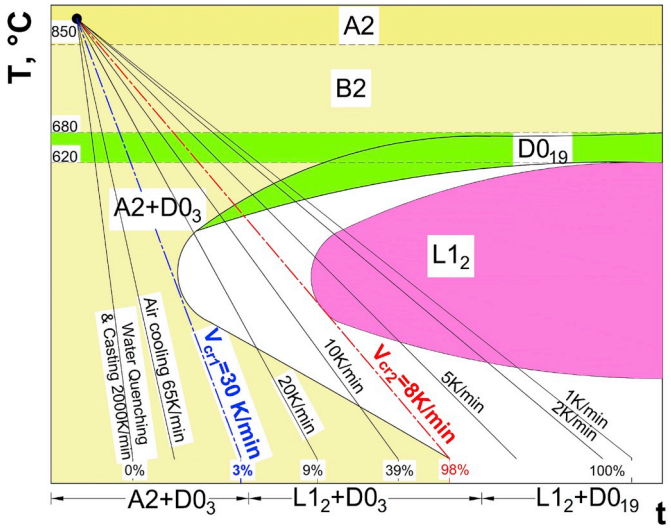

Fig. 6. Scheme of temperature – time – transition (TTT) diagram for Fe-27Ga alloy with two critical cooling rates of 30 and 8 K/min and indication (under time scale) of final structures at room temperature for given cooling rates according to our results. Both scales – temperature and time – are presented in this scheme in arbitrary units, apart from indication of three temperatures for equilibrium transitions in this alloy at about 850, 680 and 620 °C according to phase diagram [9].

the lattice parameters of the matrix and the clusters exists. A very small (~0.0002 Å), close to the statistical error, but a reliable difference is observed between their lattice parameters. This difference is smaller than the values presented in several articles on the splitting of the A2 and D0$_3$ peaks observed in the ribbons in synchrotron experiments [3,21].

In agreement with [19], the analysis of the dependence of the superstructure peak width on the *d* spacing (Williamson-Hall plot) allows estimating the size of the ordered clusters. For the samples of the first group ($15.5 \le x \le 19.5$), the size of coherently scattering domains is large and the level of microstresses is low. Starting with the composition with $x = 20.7$, the superstructure peaks appear with the width pronouncedly greater as compared to fundamental ones and correspond to the size of the ordered clusters of about $L \approx 300$ Å. For $x > 19.5$, the widths of the fundamental peaks remain almost unchanged, whereas a large size effect is seen in the widths of the superstructure peaks. Up to $x = 23.8$, three different dependences are observed in the widths of the peaks (Fig. 3), but for larger x, there remains a linear relationship for the fundamental peaks and a parabolic one for the superstructure peaks.

This means that small clusters of both B2 and D0$_3$ phases appear, whereas for $x > 24$ only D0$_3$ clusters remain. At approximately the same x value, the cluster size is stabilized (Fig. 4a).

These results indicate correlation between structure of the alloys with their magnetostriction (Fig. 4b). After nearly linear increase in both lattice parameter and magnetostriction (up to $x = 19$), decrease in both values take place up to $x = 23$ due to increase in ordering and growth of D0$_3$ clusters' size. Degree of order (intensity of the 111 peak in Fig. 3a) reaches maximum at $x \approx 24$–26, then the D0$_3$ order starts to transform gradually to B2 order. Above $x = 27$ the B2 ordering becomes dominating, which leads to decrease in magnetostriction as B2 phase is known to be paramagnetic at RT. In addition, at $x > 30$ a new phase with unresolved in this paper structure appears: according to Ref. [8], this can be paramagnetic M or R phase.

In contrast with the as cast and air-cooled samples, *the slowly cooled* in the furnace samples (the cooling rate of 2 K/min from 850 to 250 °C, then slower natural cooling in the furnace) also exhibit several groups (Fig. 2c) but with other structures:

1 $x < 19$, A2 structure.
2 $19 < x < 22$, A2 as a matrix with D0$_3$ clusters.
3 $22 < x < 25$, D0$_3$ structure with A1 or L1$_2$ precipitates.
4 $25 < x < 30$, L1$_2$ structure with retaining A3 or D0$_{19}$ phase.
5 $30 < x$, D0$_3$ structure with A1 or L1$_2$ contamination, also several

Table 1
Critical cooling rates for Fe-27Ga alloy.

	V_{Cr1}, K/min Beginning of formation of the equilibrium L1$_2$ phase out from metastable D0$_3$ phase	V_{Cr2}, K/min End of formation of equilibrium L1$_2$ phase out from metastable D0$_3$ phase
Fe-27%Ga	~30	5–8

new unresolved phases appear, probably like Fe_6Ga_5 [8].

Thus, the equilibrium $L1_2$ phase along with some amount of $D0_{19}$ phase appear in the samples with $25 < x < 30$ cooled down in the furnace with the cooling rate of 2 K/min. The lattice parameter values of these phases are not shown in Fig. 2c.

High-resolution ND patterns for two alloys after furnace cooling are shown in Fig. 5. In contrast with the as cast and air-cooled state, the furnace cooled Fe-19.5%Ga sample demonstrates $D0_3$ ordering (Fig. 5a). The structure of the furnace cooled Fe-26.9%Ga sample, as well as of the samples with higher Ga content, exhibits no sign of metastable the $D0_3$ phase but a mixture of the $L1_2$ and $D0_{19}$ phases (Fig. 5b).

Fe-26.9%Ga sample was additionally cooled down from 900 °C with well-controlled (above 250 °C) cooling rates from 1 to 30 K/min. Sample structures were examined to identify the first and second critical cooling rates (see scheme of time-temperature-transformation (TTT) diagram in Fig. 6).

The first critical cooling rate, V_{Cr1}, is defined in this paper as the cooling rate of beginning of the appearance of the equilibrium $L1_2$ phase out from the metastable $D0_3$ phase, and the second critical cooling rate, V_{Cr2}, is the cooling rate at which no metastable phase (A2, B2 or $D0_3$) is fixed in the sample structure at cooling. The results are given in Table 1. More details on phase transitions in this alloy can be found in [23].

4. Conclusions

To sum up, in this paper we (i) have analysed structure of the Fe-(9–33)at.%Ga alloys after several cooling rates and (ii) identified two critical cooling rates for Fe-27%Ga composition with respect to the beginning and end of formation of equilibrium at room temperature $L1_2$ phase. From the viewpoint of crystallographic structure, samples after casting, water quenching (cooling rate about 2000 K/min) and air cooling (60–70 K/min) have the same or very similar structure for all studied alloys. These cooling regimes prevent formation of closed packed structures (equilibrium $L1_2$ and metastable $D0_{19}$) at room temperature. It is notable, that formation of different structures at RT in as cast samples (A2 → A2 + $D0_3$ → $D0_3$ + B2 → B2 + unresolved phase with increase in Ga content in Fe–Ga alloys) correlates well and explains change in alloy magnetistriction. In the case of furnace cooling (2 K/min), samples with $x < 22\%$ have also similar structure with as quenched samples (mixture of A2 and $D0_3$ phases), while for $x > 22\%$ furnace cooling leads to the formation of closed packed $L1_2$ – dominating equilibrium at RT phase, and some tracks of $D0_{19}$ phase. Moreover, for $25 < x < 30\%$ the bcc-derived phases (A2, B2 and $D0_3$) disappear from the structure of furnace cooled samples.

Conflicts of interest

We confirm that there are no known conflicts of interest associated with this publication.

Acknowledgements

This work was supported by the Russian Science Foundation (project No. 19-72-20080). The experiments were carried out using the IBR-2 (JINR) neutron source. We are grateful to Dr. E.M. Bazanova for critical reading of this manuscript.

References

[1] A.E. Clark, J.B. Restorff, M. Wun-Fogle, T.A. Lograsso, D.L. Schlagel, Magnetostrictive properties of body-centered cubic Fe-Ga and Fe-Ga-Al alloys, IEEE Trans. Magn. 36 (2000) 3238–3240, https://doi.org/10.1109/20.908752.
[2] J. Atulasimha, A.B. Flatau, A review of magnetostrictive iron-gallium alloys, Smart Mater. Struct. 20 (2011) 043001, https://doi.org/10.1088/0964-1726/20/4/043001.
[3] Z. Nie, Z. Wang, Y. Liang, D. Cong, G. Li, C. Zhu, C. Tan, X. Yu, Y. Ren, Y. Wang, Structural investigations of Fe-Ga alloys by high-energy x-ray diffraction, J. Alloy. Comp. 763 (2018) 223–227, https://doi.org/10.1016/J.JALLCOM.2018.05.327.
[4] Y. He, Y. Han, P. Stamenov, B. Kundys, J.M.D. Coey, C. Jiang, H. Xu, Investigating non-Joulian magnetostriction, Nature 556 (2018) E5–E7, https://doi.org/10.1038/nature25780.
[5] J. Gou, X. Liu, C. Zhang, G. Sun, Y. Shi, J. Wang, H. Chen, T. Ma, X. Ren, Ferromagnetic composite with stress-insensitive magnetic permeability: compensation of stress-induced anisotropies, Phys. Rev. Mater. 2 (2018) 114406, https://doi.org/10.1103/PhysRevMaterials.2.114406.
[6] I.S. Golovin, A.M. Balagurov, Structure Induced Anelasticity in Iron Intermetallic Compounds and Alloys, Materials Research Forum LLC, USA, 2018.
[7] M. Matyunina, M. Zagrebin, V. Sokolovskiy, V. Buchelnikov, *Ab initio* study of magnetic and structural properties of Fe-Ga alloys, EPJ Web Conf. 185 (2018) 04013, https://doi.org/10.1051/epjconf/201818504013.
[8] T. Gödecke, W. Köster, UEber den Aufbau des Systems Eisen-Gallium zwischen 10 und 50 At.-% Ga und dessen Abhaengigkeit von der Waermebehandlung. II. Das Gleichgewichtsdiagramm, Z. Met. 68 (1977) 661–666.
[9] O. Kubaschewski, IRON—Binary Phase Diagrams, Springer Berlin Heidelberg, Berlin, Heidelberg, 1982, https://doi.org/10.1007/978-3-662-08024-5.
[10] T.B. Massalski, Binary Alloy Phase Diagrams, second ed., ASM International, Ohio, USA, 1990.
[11] M.V. Matyunina, M.A. Zagrebin, V.V. Sokolovskiy, O.O. Pavlukhina, V.D. Buchelnikov, A.M. Balagurov, I.S. Golovin, Phase diagram of magnetostrictive Fe-Ga alloys: insights from theory and experiment, Phase Transitions 92 (2019) 101–116, https://doi.org/10.1080/01411594.2018.1556268.
[12] O. Ikeda, R. Kainuma, I. Ohnuma, K. Fukamichi, K. Ishida, Phase equilibria and stability of ordered b.c.c. phases in the Fe-rich portion of the Fe-Ga system, J. Alloy. Comp. 347 (2002) 198–205, https://doi.org/10.1016/S0925-8388(02)00791-0.
[13] I.S. Golovin, A.M. Balagurov, V.V. Palacheva, I.A. Bobrikov, V.B. Zlokazov, In situ neutron diffraction study of bulk phase transitions in Fe-27Ga alloys, Mater. Des. 98 (2016) 113–119, https://doi.org/10.1016/j.matdes.2016.03.016.
[14] I.S. Golovin, V.V. Palacheva, D. Mari, G. Vuillème, A.M. Balagurov, I.A. Bobrikov, J. Cifre, H.-R. Sinning, Mechanical spectroscopy as an in situ tool to study first and second order transitions in metastable Fe-Ga alloys, J. Alloy. Comp. 790 (2019) 1149–1156, https://doi.org/10.1016/J.JALLCOM.2019.03.264.
[15] V.V. Palacheva, A. Emdadi, F. Emeis, I.A. Bobrikov, A.M. Balagurov, S.V. Divinski, G. Wilde, I.S. Golovin, Phase transitions as a tool for tailoring magnetostriction in intrinsic Fe-Ga composites, Acta Mater. 130 (2017) 229–239, https://doi.org/10.1016/j.actamat.2017.03.049.
[16] I.S. Golovin, A.M. Balagurov, V.V. Palacheva, A. Emdadi, I.A. Bobrikov, V.V. Cheverikin, A.S. Prosviryakov, S. Jalilzadeh, From metastable to stable structure: the way to construct functionality in Fe-27Ga alloy, J. Alloy. Comp. 751 (2018) 364–369, https://doi.org/10.1016/j.jallcom.2018.04.127.
[17] S.U. Jen, Y.Y. Lo, L.W. Pai, Temperature dependence of mechanical properties of the Fe81Ga19(Galfenol) alloy, J. Phys. D Appl. Phys. 49 (2016), https://doi.org/10.1088/0022-3727/49/14/145004.
[18] A.M. Balagurov, Scientific reviews: high-resolution fourier diffraction at the IBR-2 reactor, Neutron News 16 (2005) 8–12, https://doi.org/10.1080/10446830500454346.
[19] A.M. Balagurov, I.S. Golovin, I.A. Bobrikov, V.V. Palacheva, S.V. Sumnikov, V.B. Zlokazov, Comparative study of structural phase transitions in bulk and powdered Fe-27Ga alloy by real-time neutron thermodiffractometry, J. Appl. Crystallogr. 50 (2017) 198–210, https://doi.org/10.1107/S1600576716020045.
[20] C.J. Quinn, P.J. Grundy, N.J. Mellors, The structural and magnetic properties of rapidly solidified $Fe100-xGax$ alloys, for $12.8 \leq x \leq 27.5$, J. Magn. Magn. Mater. 361 (2014) 74–80, https://doi.org/10.1016/J.JMMM.2014.02.004.
[21] M. Huang, T.A. Lograsso, Short range ordering in Fe-Ge and Fe-Ga single crystals, Appl. Phys. Lett. 95 (2009) 10–13, https://doi.org/10.1063/1.3254249.
[22] Q. Xing, Y. Du, R.J. McQueeney, T.A. Lograsso, Structural investigations of Fe-Ga alloys: phase relations and magnetostrictive behavior, Acta Mater. 56 (2008) 4536–4546, https://doi.org/10.1016/j.actamat.2008.05.011.
[23] I.S. Golovin, A.K. Mohamed, V.V. Palacheva, V.V. Cheverikin, A.V. Pozdnyakov, V.V. Korovushkin, A.M. Balagurov, I.A. Bobrikov, N. Fazel, M. Mouas, J.-G. Gasser, F. Gasser, P. Tabary, Q. Lan, A. Kovacs, S. Ostendorp, R. Hubek, S. Divinski, G. Wilde, Comparative study of structure and phase transitions in Fe-(25-27)%Ga alloys, J. Alloys Comp 811 (2019) 152030 30 November.